Towards Automatic Power Battery Detection:
New Challenge, Benchmark Dataset and Baseline

Xiaoqi Zhao[1,2†], Youwei Pang[1,2†], Zhenyu Chen[1], Qian Yu[1],
Lihe Zhang[1*], Hanqi Liu[2], Jiaming Zuo[2*], Huchuan Lu[1]
[1]Dalian University of Technology   [2]X3000 Inspection Co., Ltd
{zxq, lartpang, dlutczy, ms.yuqian}@mail.dlut.edu.cn, {jerry, klaus}@3000gy.com
{zhanglihe, lhchuan}@dlut.edu.cn

1. Evaluation Metrics

There are eight metrics used in this work, as follows:

$$MAE_{num}^{anode} = \frac{1}{N} \sum_{i=1}^{N} \left| n_i^{anode} - \widehat{n}_i^{anode} \right|, \quad (1)$$

$$MAE_{num}^{cathode} = \frac{1}{N} \sum_{i=1}^{N} \left| n_i^{cathode} - \widehat{n}_i^{cathode} \right|, \quad (2)$$

$$Acc_{num}^{anode} = \frac{1}{N} \sum_{i=1}^{N} 1(n_i^{anode} = \widehat{n}_i^{anode}), \quad (3)$$

$$Acc_{num}^{cathode} = \frac{1}{N} \sum_{i=1}^{N} 1(n_i^{cathode} = \widehat{n}_i^{cathode}), \quad (4)$$

$$Acc_{num}^{pair} = \frac{1}{N} \sum_{i=1}^{N} 1(n_i^{pair} = \widehat{n}_i^{pair}), \quad (5)$$

$$MAE_{position}^{anode} = \frac{1}{N} \sum_{i=1}^{N} \left(\frac{1}{n_i^{anode}} \sum_{j=1}^{n_i^{anode}} \left| p_{i,j}^{anode} - \widehat{p}_{i,j}^{anode} \right| \right), \quad (6)$$

$$MAE_{position}^{cathode} = \frac{1}{N} \sum_{i=1}^{N} \left(\frac{1}{n_i^{cathode}} \sum_{j=1}^{n_i^{cathode}} \left| p_{i,j}^{cathode} - \widehat{p}_{i,j}^{cathode} \right| \right), \quad (7)$$

$$MAE_{overhang}^{pair} = \frac{1}{N} \sum_{i=1}^{N} \left(\frac{1}{n_i^{cathode}} \sum_{j=1}^{n_i^{cathode}} \left| (|p_{i,j}^{cathode} - p_{i,j}^{anode}| + |p_{i,j}^{cathode} - p_{i,j+1}^{anode}|) - (|\widehat{p}_{i,j}^{cathode} - \widehat{p}_{i,j}^{anode}| + |\widehat{p}_{i,j}^{cathode} - \widehat{p}_{i,j+1}^{anode}|) \right| \right), \quad (8)$$

---

† Equal contribution.
∗ Corresponding author.

Method	AN-MAE↓	CN-MAE↓	AN-ACC↑	CN-ACC↑	PN-ACC↑	AL-MAE↓	CL-MAE↓	OH-MAE↓
Baseline	2.3892	1.4782	0.5363	0.5741	0.5141	3.8171	3.0830	3.3911
+ PFM	1.2320	0.7389	0.6467	0.7035	0.6340	3.5168	2.8312	3.1730
+ CP	0.8342	0.3782	0.6971	0.7981	0.6909	3.4143	2.7320	3.0311
+ LP	0.4259	0.2050	0.7855	0.9306	0.7603	2.4397	2.0978	2.1092

Table 1. Ablation experiments of each component in the MDCNet on the difficult split.

Method	AN-MAE↓	CN-MAE↓	AN-ACC↑	CN-ACC↑	PN-ACC↑	AL-MAE↓	CL-MAE↓	OH-MAE↓
Baseline	4.3223	3.3240	0.2989	0.4138	0.2586	3.7476	3.1356	3.6235
+ PFM	3.1349	2.6393	0.4253	0.5172	0.3793	3.6354	3.0325	3.5012
+ CP	2.4763	2.1223	0.4885	0.6034	0.4483	3.6255	2.9222	3.3521
+ LP	2.0920	1.8966	0.5632	0.6839	0.5115	2.0004	1.4654	1.6291

Table 2. Ablation experiments of each component in the MDCNet on the tough split.

where N is the scale of the test dataset, n_i^x and $\widehat{n}_i^x$ separately represent the number of predicted plates and ground truth plates for the ith sample ($x \in \{anode, cathode, pair\}$), $p_{i,j}^y$ and $\widehat{p}_{i,j}^y$ separately represent the position coordinates of the jth predicted plate and ground truth plate for the ith sample ($y \in \{anode, cathode\}$). We need to sort the coordinates of the plates before calculating $MAE_{position}^{anode}$, $MAE_{position}^{cathode}$ and $MAE_{overhang}^{pair}$.

Generally, the corresponding n_i^x can be obtained by counting the number of $p_{i,j}^y$. Corner detection methods directly predict the coordinate value of each endpoint. General/Tiny object detection methods predict the bounding box for each endpoint, and we utilize the box to calculate the center coordinates as $p_{i,j}^y$. Counting methods obtain the n_i^x by accumulating the spatial values of the predicted density maps. Our segmentation-based MDCNet can predict each point map, and we obtain the coordinate of the endpoint by calculating the center coordinates for the circumscribed rectangle of each point map.
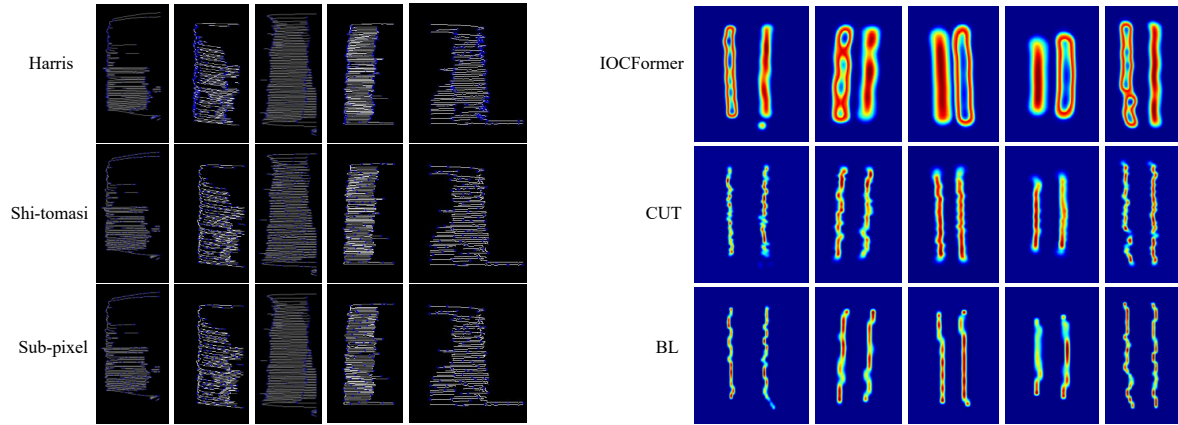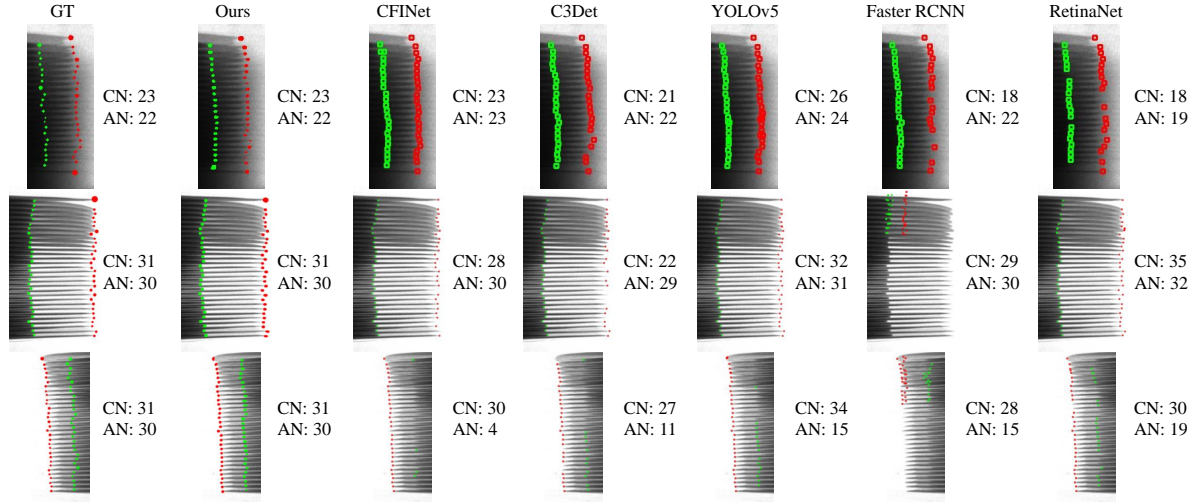
1

Figure 1. Visual comparison with other methods.

Method	AN-MAE↓	CN-MAE↓	AN-ACC↑	CN-ACC↑	PN-ACC↑	AL-MAE↓	CL-MAE↓	OH-MAE↓
Const-1	3.1556	2.4758	0.4101	0.4479	0.3722	2.5875	2.5312	2.4578
Const-3	2.4310	1.7563	0.6467	0.6940	0.5868	2.5461	2.4277	2.4006
Const-5	2.4315	1.7563	0.6309	0.6940	0.5836	2.5565	2.2899	2.3973
Ada-0.1	2.8562	2.0223	0.5521	0.6625	0.4890	2.4435	2.1544	2.2654
Ada-0.3	0.4259	0.2050	0.7855	0.9306	0.7603	2.4397	2.0978	2.1092
Ada-0.5	0.9785	0.6876	0.7035	0.8486	0.6688	2.5851	2.2954	2.3025

Table 3. Quantitative comparison of different label generation strategies and settings for the point segmentation branch on the difficult split.

Method	AN-MAE↓	CN-MAE↓	AN-ACC↑	CN-ACC↑	PN-ACC↑	AL-MAE↓	CL-MAE↓	OH-MAE↓
Const-1	6.5420	5.4246	0.1724	0.2356	0.1207	2.5854	1.9462	2.0996
Const-3	4.0102	3.4432	0.4195	0.4943	0.3621	2.3844	1.7215	1.9235
Const-5	4.0674	3.4432	0.4023	0.4943	0.3506	2.3457	1.6947	1.9021
Ada-0.1	5.4123	4.0215	0.2874	0.3736	0.2586	2.3526	1.6785	1.8645
Ada-0.3	2.0920	1.8966	0.5632	0.6839	0.5115	2.0004	1.4654	1.6291
Ada-0.5	2.2147	2.0456	0.4828	0.5402	0.4023	2.1756	1.5455	1.7442

Table 4. Quantitative comparison of different label generation strategies and settings for the point segmentation branch on the tough split .

2. Ablation Study

Tab. 1 - Tab. 6 list the results of ablation study on the difficult and tough splits, which can show the effectiveness of each component in the multi-dimensional collaborative network, label generation strategies and the strong stability of the prompt filter module.

3. Qualitative Evaluation

Fig. 1 illustrates the visual comparison of general/tiny object detection-based solutions, corner detectors and couting methods with our segmentation-based MDCNet. We directly visualize the predicted results (MDCNet: Segmentation map, Others: Bounding box, Corner map, Density

No.	AN-MAE↓	CN-MAE↓	AN-ACC↑	CN-ACC↑	PN-ACC↑	AL-MAE↓	CL-MAE↓	OH-MAE↓
1	0.4259	0.2050	0.7855	0.9306	0.7603	2.4397	2.0978	2.1092
2	0.4259	0.2050	0.7855	0.9306	0.7603	2.4397	2.0978	2.1092
3	0.4259	0.2050	0.7855	0.9306	0.7603	2.4397	2.0978	2.1092
4	0.4259	0.2050	0.7855	0.9306	0.7603	2.4397	2.0978	2.1092
5	0.4259	0.2050	0.7855	0.9306	0.7603	2.4397	2.0978	2.1092

Table 5. Evaluation of the PFM with different prompt inputs on the difficult split.

No.	AN-MAE↓	CN-MAE↓	AN-ACC↑	CN-ACC↑	PN-ACC↑	AL-MAE↓	CL-MAE↓	OH-MAE↓
1	2.0920	1.8966	0.5632	0.6839	0.5115	2.0004	1.4654	1.6291
2	2.0920	1.8966	0.5632	0.6839	0.5115	2.0004	1.4654	1.6291
3	2.0920	1.8966	0.5632	0.6839	0.5115	2.0004	1.4654	1.6291
4	2.0920	1.8966	0.5632	0.6839	0.5115	2.0004	1.4654	1.6291
5	2.0920	1.8966	0.5632	0.6839	0.5115	2.0004	1.4654	1.6291

Table 6. Evaluation of the PFM with different prompt inputs on the tough split.

map) without any post-processing operations. It can be seen that the proposed method yields the results closer to the ground truth in various challenging scenarios. Other methods often suffer from missed and repeated detection failures. Especially for samples with indistinct cathode features, detection methods based on a single two-dimensional box supervision form consistently perform poorly (see the 3th row). Although we have performed edge extraction to pre-filter a large amount of background irrelevant to plate endpoints, these corner detectors still introduce a lot of redundancy and can not distinguish plate endpoints from general intersection points. Density maps usually provide the rough body location of the plates but can not explicitly obtain the coordinates of each plate one by one without applying any post-processing techniques.